ACS APPLIED MATERIALS & INTERFACES

Research Article

www.acsami.org

Silica Nanoparticles Treated by Cold Atmospheric-Pressure Plasmas Improve the Dielectric Performance of Organic−Inorganic Nanocomposites

Wei Yan,[†,‡] Zhao Jun Han,[‡] B. Toan Phung,[†] and Kostya (Ken) Ostrikov*[,‡,§]

[†]School of Electrical Engineering and Telecommunications, The University of New South Wales, Sydney, NSW 2052, Australia
[‡]Plasma Nanoscience Centre Australia (PNCA), CSIRO Materials Science and Engineering, Lindfield, NSW 2070, Australia
[§]Plasma Nanoscience, Complex Systems, School of Physics, The University of Sydney, Sydney, NSW 2006, Australia

Supporting Information

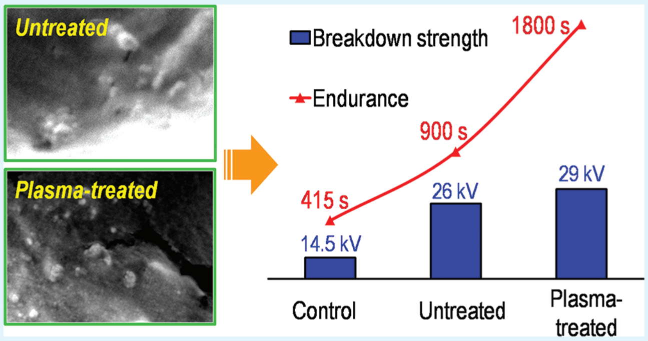

ABSTRACT: We report on the application of cold atmospheric-pressure plasmas to modify silica nanoparticles to enhance their compatibility with polymer matrices. Thermally nonequilibrium atmospheric-pressure plasma is generated by a high-voltage radio frequency power source operated in the capacitively coupled mode with helium as the working gas. Compared to the pure polymer and the polymer nanocomposites with untreated SiO_2, the plasma-treated SiO_2−polymer nanocomposites show higher dielectric breakdown strength and extended endurance under a constant electrical stress. These improvements are attributed to the stronger interactions between the SiO_2 nanoparticles and the surrounding polymer matrix after the plasma treatment. Our method is generic and can be used in the production of high-performance organic−inorganic functional nanocomposites.

KEYWORDS: *organic−inorganic nanocomposites, atmospheric pressure plasma, insulation, partial discharge, dielectric breakdown*

INTRODUCTION

The incorporation of inorganic nanoparticles into polymer matrices is very promising to improve the properties of organic−inorganic nanocomposites, which are considered very attractive materials for the development of next-generation, high-performance devices for numerous advanced applications.[1−7] One of these applications is high-voltage insulation, where polymer-based organic−inorganic nanocomposites have shown major advantages (e.g., flexibility, processability, good performance, low weight, low cost, etc.) over the conventional insulation materials.[7] SiO_2, TiO_2, and Al_2O_3 are among the most-widely used inorganic nanoparticles to be filled in the dielectric polymers. However, a common problem associated with these nanoparticles is that they often tend to agglomerate because of surface incompatibility between the inorganic fillers and the polymer matrices. As such, the insulation performance of these nanocomposites is often substantially degraded.

Using a coupling agent to modify the surface of nanoparticles prior to mixing them with polymers has been attempted in both laboratories and industries.[8] Grafting of organic groups (e.g., amine or silane) on the nanoparticle surfaces has been demonstrated to improve the dispersion uniformity in the polymer matrices.[9,10] However, the low surface reactivity of these nanoparticles often inhibits strong interactions between the nanoparticles and the surrounding polymers, resulting in unsatisfactory improvements of the properties of the nanocomposites.

To resolve these issues, here we use thermally nonequilibrium, cold atmospheric-pressure plasmas to modify the surface of the nanoparticle fillers. We show that the plasma-surface reactions can effectively increase the surface energy and the reactivity of these nanoparticles. This in turn results in a better dispersity and stronger interactions with the polymer matrices. Compared to their untreated counterparts, the plasma-treated nanocomposites therefore attain higher dielectric breakdown strength and also longer endurance under the constant electrical stress. These results demonstrate a simple yet effective technique to improve the physical and chemical properties of the functional organic−inorganic nanocomposites, thereby advancing their applications in many fields.

EXPERIMENTAL SECTION

Materials. Hydrophobic fumed silica nanoparticles grafted with dimethyldichlorosilane (DDS) were provided by Evonik Industries, Germany. The nanoparticles had an average particle size of 16 nm and a surface area of 110 m^2/g. The epoxy resin (RX771C/NC) containing bisphenol A diglycidyl ether (BADGE) was obtained from ROBNOR

Received: February 21, 2012
Accepted: April 10, 2012
Published: April 10, 2012

RESINS Ltd. The curing agent (ARADUR HY 1300 GB) consisted of triethylenetetramine (TETA) was supplied by Huntsman Advanced Materials. This thermoset epoxy resin has been widely used as insulation materials in high-voltage applications.[11]

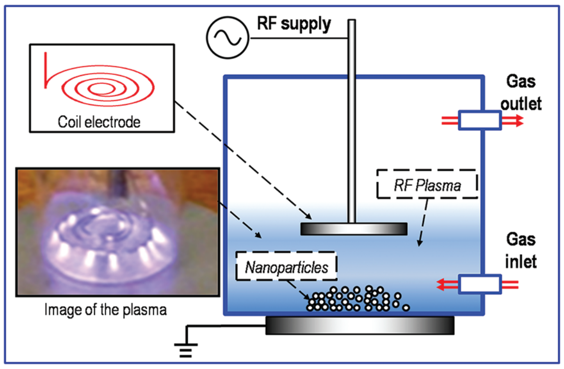

Figure 1. Setup of the atmospheric-pressure plasma reactor. The bottom wall of the bottle serves as a dielectric barrier. During the treatment, the nanoparticles were placed in the uniform plasma zone and exposed to the plasma. Inset (top) shows the schematic of a coil electrode placed 5 mm above the bottom of the glass bottle. Inset (bottom) shows a real-time photograph of the plasma discharge.

Atmospheric-Pressure Plasma Treatment. The surface modification of the as-received silica nanoparticles was carried out in a custom-designed atmospheric-pressure plasma reactor (Figure 1). Cold atmospheric-pressure plasma was generated by a 350 kHz radio frequency (RF) power supply with a maximum 5 kV peak-to-peak output. A tin-coated copper coil electrode was placed 2 mm above the top of the nanoparticle layer. The ground electrode was placed under the reactor to form a dielectric barrier discharge (DBD) structure.[12] Helium was used as the working gas for the discharge. The plasma was generated by a 4 kV peak-to-peak RF voltage (the voltage and current waveforms are shown in Figure S1 in the Supporting Information). The power density in the plasma region was estimated to be 60 mW/cm^3.[13−16]

In each experiment, we have put 50 mg of the nanoparticles on the bottom of the reactor. These particles formed an evenly distributed, 3 mm thick soft layer. As the outer diameter of the coil was close to the diameter of the cylindrical reactor, the plasma zone generated by the coil electrode can fully cover the whole surface of the nanoparticle layer (also see the inset of Figure 1). We also observed that the plasma can partially penetrate the thin nanoparticle layer and reach the bottom layer of the nanoparticles during the experiments. Moreover, the nanoparticles remained powder-like and no clear changes in the morphology of the nanoparticle layer were found after the plasma treatment. Occasionally, however, it was noted that the treated particles tended to attach to the wall of the reactor.

To obtain a fairly uniform exposure, the nanoparticles were first treated by the atmospheric-pressure plasma for 5 min; the plasma was then stopped and the nanoparticles were stirred using a magnetic bar for 10 s. This treatment-stirring process was repeated 6 times and the total treatment time of the nanoparticles was 30 min.

Synthesis of Polymer Nanocomposites. First, 0.71 g of curing agent was added into 1.79 g of epoxy resin to obtain a 4:10 weight ratio. High-speed mechanical stirring was continuously performed to obtain a uniform fluid. Due to the high viscosity of the fluid, 0.05 g of SiO_2 nanoparticles were dispensed into the resin in three batches, with an interval of 10 min. After being stirred for 40 min, the mixture was degassed for 1 h under vacuum (<100 Pa) until no bubbles were observed. The mixture was then poured into a premade cylindrical mold. A tungsten needle with the tip curvature of 1.3 μm was embedded vertically into the nanocomposites for testing the electrical insulation performance (see Figure S2 in the Supporting Information). After that, the mold was annealed at 40 °C for 2 h, followed by curing at room temperature for another 48 h. The fabricated nanocomposites with untreated and plasma-treated SiO_2 were denoted as UTNCs and PTNCs, respectively. Pure epoxy resin as a control sample was also fabricated and denoted as PER.

Insulation Performance Tests. The partial discharge (PD) characteristic is one of the most important parameters for evaluating the performance of an insulation material as the development of PD causes the degradation to the material and eventually leads to the ultimate breakdown.[7] The PD measurements were performed using OMICRON MPD600 PD detection unit with the measurement circuit shown in Figure S3 in the Supporting Information. This circuit included a 1000 pF blocking capacitor (C_b) and a detection impedance (Z). The discharge-free detection system was powered by a high-voltage power supply. Each sample was placed in a test cell filled with insulation oil to avoid any unwanted surface discharge (see Figure S4 in the Supporting Information). The maximum voltage that could be achieved in this system was 50 kV at 50 Hz.

In our measurements, a voltage was ramped from 0 V up until the occurrence of an ultimate breakdown to obtain the inception voltage and the dielectric breakdown strength of each sample. The PD inception threshold was set as 10 pC. Additionally, an endurance test under a sustained AC voltage was performed using the same circuit as in the PD measurements, except that the frequency was adjusted to 300 Hz to speed up the aging effect as compared to the 50 Hz power frequency. The applied root-mean-square (rms) voltage for the endurance test V_{endu} was 7.5 kV.

Material Characterizations. X-ray photoelectron spectroscopy (XPS) spectra were obtained in both survey and narrow-scan modes using the SAGE150 Compact ESCA System (SPECS) with a monochromatic Mg $K\alpha$ radiation at 1253.6 eV. The detected spot size of the samples was 1 × 2 mm^2. A Gaussian−Lorentzian (30/70) product function was used for XPS peak deconvolutions. For sample preparation, nanoparticles were first transferred onto a molybdenum sheet, followed by dropping one drop of ethanol. Upon the drying of ethanol, uniform and flat layers of both untreated and plasma-treated nanoparticles were obtained with a good surface coverage. In this way, the contribution from the silica nanoparticles in the XPS spectra was minimized. Field emission scanning electron microscopy (FESEM) images was obtained using a Zeiss Ultra Plus microscope with an electron beam energy of 15 keV. For the SEM imaging, the nanoparticle samples were prepared by directly placing them onto a carbon adhesive tape. In contrast, the nanocomposite samples were viewed by scraping the thin cross-section sheets from the bulk material. Both samples were decorated with gold to prevent surface charging in SEM observations.

Electric Field Simulation. To study the effect of nanoparticle agglomeration on the uniformity of electric field in their vicinity, a simulation was carried out using the Maxwell-2D software.[17] Specifically, a sphere model was used as the agglomerated nanoparticles in the simulation. Spheres with different diameters were placed in a homogeneous electric field to show the correlation between the agglomeration size and the intensity of the distorted electric field.

■ RESULTS AND DISCUSSION

Plasma-Treated Nanocomposites. Atmospheric-pressure plasmas are widely used in surface modification and activation on organic substrates as a variety of reactive species can be generated at room temperature.[18,19] In our experiments, we used the atmospheric-pressure plasma to modify silane-functionalized SiO_2 nanoparticles. It was noted that nanoparticles were partially suspended in the plasma during the process, an effect that was very similar to dusty plasmas where the nonagglomeration is reached by electrical charging.[20,21] We expected that the Si−C and Si−O bonds in the surface silane groups can be broken due to the energetic ions in the plasma. This can further create activated surface sites to form chemical bonds with the surrounding polymer matrix after the nanoparticles were added into the polymer host.

Figure 2 shows the Si 2p XPS spectra of both the untreated and the plasma-treated SiO_2 nanoparticles. From this figure, one can see that the whole Si 2p spectrum has shifted from a higher binding energy (BE), as in the case of the untreated nanoparticles, to a lower BE after the plasma treatment. The surface of untreated SiO_2 nanoparticles featured both Si–C and Si–O bonds (see Figure S5 in the Supporting Information). Because of the presence of highly reactive species and energetic particles (such as excited radicals, molecules, atoms, O, O^+,O_2^+, NO, etc.) in the atmospheric-pressure plasmas,[12,22−24] the Si–O and Si–C bonds were broken and free radicals on the surface of nanoparticles may form.[25−28] These functional and charging groups could mitigate the surface charging effect of silica nanoparticles, leading to a shift to the lower BE as observed in the XPS spectra of the treated nanoparticles. The plasma treatment may also result in the release of surface oxygen atoms and the associated reduction of the Si–O bonds. Indeed, the intensity of the XPS peak assigned to the Si–O bonds (BE ~107 eV) has decreased by 20.7% after the plasma treatment (Figure 2).

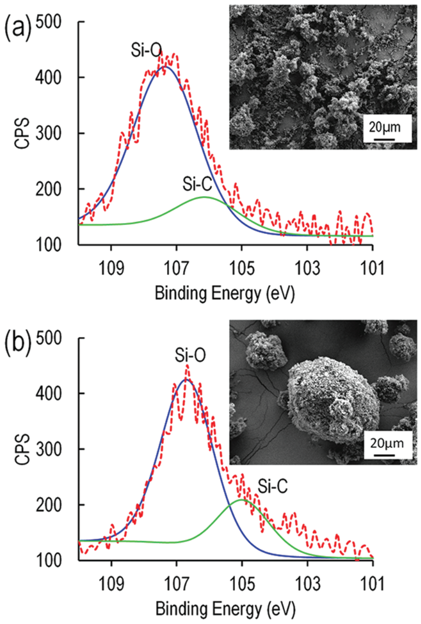

Figure 2. Surface composition and morphology of the silica nanoparticles. XPS spectra (dotted lines) with deconvoluted Si–O and Si–C bonds are shown for (a) untreated and (b) plasma-treated silica nanoparticles. Insets in (a) and (b) are the corresponding SEM images of the untreated and plasma-treated nanoparticles, respectively.

The SEM images of the untreated and treated SiO_2 nanoparticles are also shown in the insets of Figure 2. It is observed that the treated nanoparticles self-organized into quasi-spherical agglomerates with diameters ranging from 10 to 100 μm. In contrast, no obvious morphological changes were found in the untreated nanoparticles. The formation of the agglomerates was most likely due to the increased surface energy of the plasma-treated nanoparticles.[26]

The synthesized nanocomposites were further investigated when mixed with both untreated and plasma-treated silica nanoparticles. The reaction between the epoxy resin BADGE and the curing agent TETA to form the thermoset is depicted in Figure S6 in the Supporting Information. However, after the plasma-treated nanoparticles were added, a number of the TETA backbone nitrogen atoms turned to bond with the activated surface silane groups of the adjacent SiO_2 particles.[29] This resulted in the formation of Si–N bonds instead of the commonly expected C–N bonds, i.e., the epoxide groups (in the dashed boxes in Figure S6 in the Supporting Information) were replaced by the nanofillers.

To validate the formation of these bonds, the C 1s peaks of the pure epoxy resin (PER), untreated nanocomposite (UTNC), and plasma-treated nanocomposite (PTNC) are compared in Figure 3 and the concentrations of each chemical bonds are presented in Table 1. From these results, one can see that indeed the concentration of the C–N bond (around 285.7 eV) in the PER sample has decreased from 65% to 43% in the PTNC sample. On the other hand, the UTNC sample had a similar C–N concentration (69%) as in the PER sample, implying that the reaction between the untreated nanofillers and the polymer matrix was negligible. Besides, the *N 1s* peaks of both UTNC and PTNC samples showed that only one peak corresponding to the C–N bond was found in the UTNC sample, whereas an additional peak corresponding to the Si–N bond was observed in the PTNC sample (see Figure S7 in the

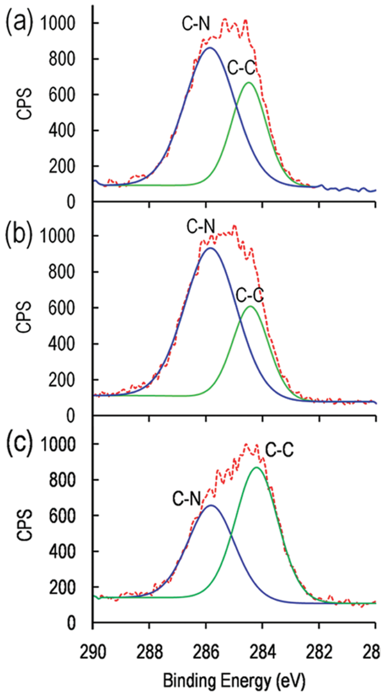

Figure 3. Surface composition of the polymer nanocomposites. XPS spectra (dotted lines) with deconvoluted C–N and C–C bonds are shown for (a) PER, (b) UTNC, and (c) PTNC samples, respectively.

Table 1. C 1s Binding Energies (BE) and Surface Concentrations from the XPS Spectra of the Pure Epoxy Resin (PER), the Untreated Nanocomposite (UTNC), and the Plasma-Treated Nanocomposite (PTNC) Samples

PER			UTNC			PTNC		
BE (eV)	concentration (%)		BE (eV)	concentration (%)		BE (eV)	concentration (%)	
283.9	**C–C**	35	283.5	**C–C**	31	283.6	**C–C**	57
285.3	**C–N**	65	284.9	**C–N**	69	285.2	**C–N**	43

Supporting Information). Furthermore, there was no apparent difference in the dispersion uniformity between the epoxy resin nanocomposites with the untreated and the plasma-treated nanoparticles (Figure 4a,b). One can thus conclude that while the plasma modification led to stronger interactions between the nanoparticles and the polymer matrices, the nanoparticle dispersion in the nanocomposites remained uniform.

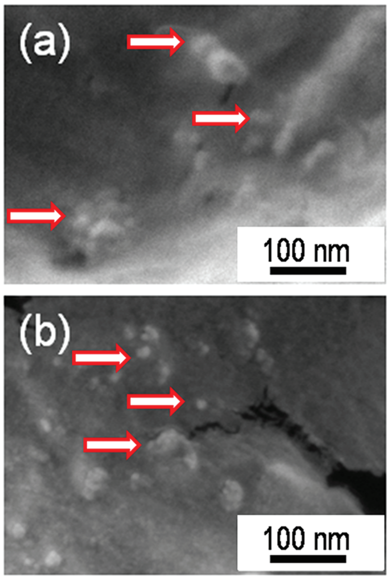

Figure 4. Surface morphology of polymer nanocomposites. Both (a) UTNC and (b) PTNC samples show good dispersion uniformity in the polymer matrices. Arrows in (a) and (b) point to the embedded SiO_2 nanoparticles.

Dielectric Properties. We then investigated the partial discharge (PD) and the ultimate dielectric breakdown phenomena which characterize the initial and final stage of the dielectric fault process for insulation materials.[30] Figure 5 shows the PD inception voltage, the breakdown voltage, and the PD withstanding time against the ramped voltage for all three samples. One can see that both UTNC and PTNC samples showed a significant increase in their PD inception and breakdown voltage as compared to those of the PER sample. This result features the effectiveness of SiO_2 nanofillers in improving the PD resistivity and the insulation strength. Moreover, the UTNC showed a higher tolerance to the electrical stress before the partial discharge occurred (21.4 kV), whereas the PTNC revealed the highest dielectric breakdown strength (29 kV). The slightly lower PD inception voltage of PTNC as compared to that of UTNC is presently unclear and could be due to the unavoidable nonuniformities and fluctuations during the sample preparation or electric testing processes. The significantly increased dielectric breakdown voltage of the PTNC sample is discussed in detail in the next section.

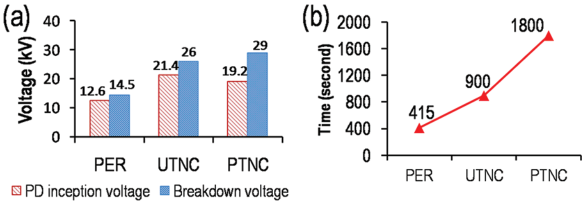

Figure 5. Dielectric performance of the polymer nanocomposites. As compared to the PER sample, both UTNC and PTNC samples show significantly improved (a) PD inception and breakdown voltages and (b) PD withstanding time.

To demonstrate the dynamics of the partial discharge process from its inception to the ultimate breakdown stage in the polymer nanocomposites, we also plotted the real-time PD level and the applied ramp voltage in Figure 6. We found that the PD withstanding time of PER was only 415 s. However, this time was extended to 900 s in the UTNC sample. A more significant increase was observed in the PTNC sample where the dielectric breakdown did not occur until 1800 s after the PD inception (Figure 5b). In addition, it was noticed that the PD level trends of the two nanocomposites (UTNC and PTNC) exhibited comb-like spectra, whereas the PER sample exhibited a smoother and monotonically increasing curve. This indicated that the PD spikes of the nanocomposites were intermittent and the PD level dropped to a very low value shortly after a single spike, confirming the ability of the produced polymer nanocomposites to recover against the partial discharge.

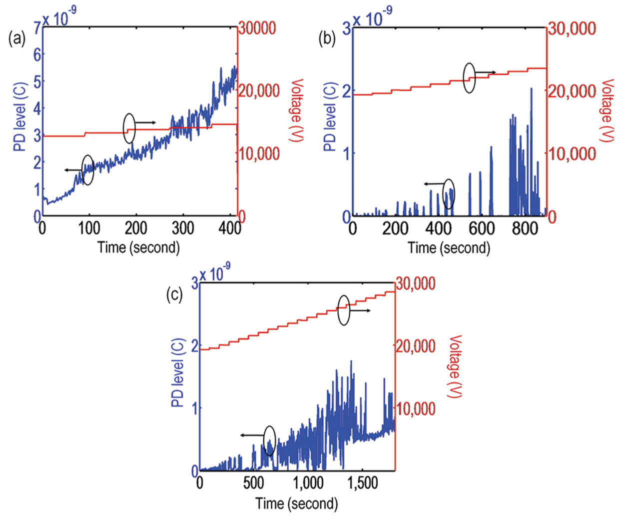

Figure 6. Real-time PD level and the applied ramp voltage of the polymer nanocomposites. The PD curves in (b) UTNC and (c) PTNC samples show comb-like spectra with multiple peaks, whereas a smooth, monotonically increasing curve is found in the (a) PER sample.

The endurance test under a critical electrical stress demonstrates the ability of insulation materials to retain a normal performance before the ultimate breakdown. In our samples, we also found that the endurance of the PTNC sample was higher than that of the UTNC sample. The lifetime of the PTNC sample was about 19 h, compared to only 14.7 h for the UTNC sample (see Figure S8 in the Supporting Information). Such a long endurance of PTNC may lead to a high stability and lower the maintenance cost of the high-voltage insulation nanocomposites. These results therefore demonstrated that the simple atmospheric-pressure plasma treatment indeed effectively improved the dielectric stability of the organic−inorganic nanocomposites.

Mechanism and Simulation. We now address the mechanism of the improved dielectric properties of the plasma-treated SiO_2-polymer nanocomposites. It is known that nanoparticle interfaces within a matrix play a very significant role in various devices, such as solar cells.[31] However, carrier recombination on such interfaces is detrimental in solar cells, whereas in insulating nanocomposites, it is beneficial as more electrons recombine to weaken the avalanche. The electrical treeing phenomenon, which determines the lifetime of an insulation material, is believed to be the main reason responsible for the ultimate breakdown in the needle-to-plane electrode geometry used in our measurements.[32] The process of electrical treeing is schematically illustrated in Figure S9 in the Supporting Information. The development of the electrical treeing involves the two phases: the void formation and the tree propagation. The former is generated in the vicinity of the tip of the needle electrode; whereas the latter occurs when many gaseous tunnels propagate toward the plane electrode. The ultimate dielectric breakdown is then induced when any of the trees link the two electrodes.[7]

There are two possible routes to form gaseous voids (the first phase of breakdown) in the nanocomposites: (1) air may remain within the material during the fabrication, and (2) gaseous byproducts generated in the process of polymer degradation. In this work, the first route was excluded as we had sufficiently degassed all the samples during the preparation stage. Therefore, the generation of gaseous byproducts can be attributed to the structural deformation of the polymeric insulation upon electron degradation, as discussed in detail below.

The electrons injected from the electrodes are accelerated in the free volume by the applied electric field; this may deform the polymer molecules.[33] The energy gain of an electron in the electric field is

$$W = eEl_x \tag{1}$$

where e is the electron charge, E is the magnitude of the applied electric field, and l_x is the mean free path of the electron before it encounters a collision. The magnitude of the applied electric field around the tip of the needle electrode can be derived according to

$$E = \frac{2V}{r\ln(4d/r)} \tag{2}$$

where r is the radius of the tip, d is the distance between two electrodes, and V is the applied voltage across the specimen. Taking the endurance test as an example, the maximum electric field around the needle tip was 1.87×10^9 V/m.

Next, we justify the value of l_x in the experiments. Although l_x can vary when inorganic nanoparticles were incorporated, previous studies indicated that such variation was only within ±5% compared to the pristine polymer.[34,35] Additionally, the distribution of l_x is found to be a combination of two Gaussian's functions (see Figure S10 in the Supporting Information), which can be expressed as[30,36−38]

$$f(x) = a_1 e^{-(x-\mu_1)^2/2\sigma_1^2} + a_2 e^{-(x-\mu_2)^2/2\sigma_2^2} \tag{3}$$

where a_1 and a_2 are constants, μ_1 and μ_2 are the means, and σ_1 and σ_2 are the standard deviations of the two individual Gaussian functions, respectively. By fitting the curve with parameters from Lim et al.,[38] one has $a_1 = 0.014$, $a_2 = 0.005$, $\sigma_1 = 0.111$, $\sigma_2 = 0.548$, and $\mu_1 = 0.6$ and $\mu_2 = 1$.

Table 2. Chemical Bonds in the Epoxy Resin and Their Corresponding Bond Dissociation Energy (BDE).[39,40]

	C−C	C−O	C−N	C−H	Si−N
bond dissociation energy (eV)	3.6	3.7	3.1	4.3	3.7

Table 2 lists the existing bonds in the nanocomposites and the corresponding bond dissociation energy (BDE).[39,40] Apparently, the C−N bond has the lowest BDE (3.1 eV) among all of them. We found that to break this C−N bond, l_x has to be larger than 1.6 nm according to eq 1. As shown in Figure S10 in the Supporting Information, about 8.8% of the total number of electrons have such mean free path. In contrast, the incorporation of the plasma-treated SiO_2 nanoparticles replaced the C−N bonds (3.1 eV) with the Si−N bonds (3.7 eV), leading to only 2.2% of the electrons with sufficient energy to break the bonds (Figure S10). The polymer molecules in the plasma-treated SiO_2 nanocomposites were therefore much more stable than those in the pristine sample. Consequently, the occurrence of the partial discharge was largely delayed,[30] as evidenced in the endurance test (see Figure S8 in the Supporting Information).

Once the initial gas voids are created, the tree "branches" propagate rapidly throughout the nanocomposite. This corresponds to the tree propagation stage in Figure S9 in the Supporting Information. At this stage, a higher PD magnitude of the PTNC than the UTNC was observed. This can be explained by the combination of uniformly distributed nanoparticles and a small number of microsized clusters in the PTNC sample. To demonstrate this clearly, we simulated the electric field distribution around SiO_2 nanoparticles of different sizes (Figure 7). The results of this simulation show that a particle of a larger size may lead to a higher partial electrical stress compared to the stress induced by the smaller ones. The overstressed regions could contribute to the propagation of the electrical tree and lead to an increased PD level. Since the origin of such effect was the unwanted agglomeration and the weak interactions between the nanofillers and the polymer matrix, the plasma treatment of nanoparticles before mixing them with the matrix shows a promising solution to this significant problem.

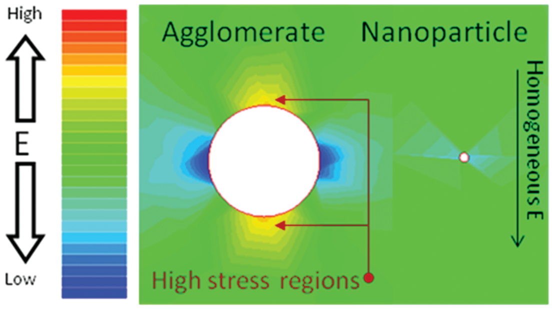

Figure 7. Simulation of the vicinal electrical stress near particles with different sizes in a homogeneous external electric field. Higher stress regions are found at the opposite poles of the large agglomerate, whereas no obvious distortion in the vicinal electrical field is observed near the small nanoparticle.

■ CONCLUSION

In summary, we have demonstrated that the cold atmospheric-pressure plasma treatment is a practical, effective and environmentally friendly method to improve the compatibility and the characteristics of the interfacial region in organic−inorganic polymer-based nanocomposite materials. This treatment produces stronger chemical bonds and also reduces the presence of weak bonds within the synthesized nanocomposite, while maintaining excellent dispersion uniformity of the nanoparticles. As a result, significant improvements of the dielectric insulation properties were found in a plasma-treated-SiO_2-filled epoxy resin nanocomposite even at a low nanoparticle loading rate. This method is generic and can be beneficial to virtually any organic−inorganic nanocomposite systems to provide higher mechanical strength, thermal stability, electrical property, etc. As such, applications in a wide range of fields, e.g., nanobiomedicine, food packaging, organic electronics and optoelectronics, and development of high-capacity energy storage devices, can benefit from this reasonably simple, inexpensive, and environmentally friendly technique.

■ ASSOCIATED CONTENT

Ⓢ Supporting Information

The voltage and current waveshapes of the plasma load. The geometry and images of molded samples for insulation tests. Partial discharge test circuit. Insulation-oil-filled test cell loaded with a sample. The surface structure of the as-received silane grafted SiO_2. Surface composition of the polymer nanocomposites. Reaction of the thermoset epoxy resin kit. Partial discharge level spectra of 7.5 kV endurance test. The electrical treeing process in the nanocomposite. The distribution density of the mean free paths l_x of the electrons in the nanocomposite. This material is available free of charge via the Internet at http://pubs.acs.org.

■ AUTHOR INFORMATION

Corresponding Author

*E-mail: kostya.ostrikov@csiro.au.

Notes

The authors declare no competing financial interest.

■ ACKNOWLEDGMENTS

The authors thank S. Kumar, Q. J. Cheng, S. Yick, and Z. Liu for helpful discussion and technical assistances. Z. J. Han acknowledges the support of OCE Postdoctoral Fellowship. This work was partially supported by the University of New South Wales, the Australian Research Council (ARC), and CSIRO's OCE Science Leadership Program.

■ REFERENCES

(1) Vendamme, R.; Onoue, S. Y.; Nakao, A.; Kunitake, T. *Nat. Mater.* **2006**, *5*, 494−501.

(2) Lu, Y. F.; Yang, Y.; Sellinger, A.; Lu, M. C.; Huang, J. M.; Fan, H. Y.; Haddad, R.; Lopez, G.; Burns, A. R.; Sasaki, D. Y.; Shelnutt, J.; Brinker, C. J. *Nature* **2001**, *410*, 913−917.

(3) Dresselhaus, M. S.; Chen, G.; Tang, M. Y.; Yang, R. G.; Lee, H.; Wang, D. Z.; Ren, Z. F.; Fleurial, J. P.; Gogna, P. *Adv. Mater.* **2007**, *19*, 1043−1053.

(4) Chattopadhyay, D. K.; Raju, K. V. S. N. *Prog. Polym. Sci.* **2007**, *32*, 352−418.

(5) Bansal, A.; Yang, H.; Li, C.; Cho, K.; Benicewicz, B. C.; Kumar, S. K.; Schadler, L. S. *Nat. Mater.* **2005**, *4*, 693−698.

(6) Abramson, A. R.; Kim, W. C.; Huxtable, S. T.; Yan, H. Q.; Wu, Y. Y.; Majumdar, A.; Tien, C. L.; Yang, P. D. *J. Microelectromech. Syst.* **2004**, *13*, 505−513.

(7) Tanaka, T. *IEEE T. Dielect. Elect. Insul.* **2005**, *12*, 914−928.

(8) Ma, D. L.; Hugener, T. A.; Siegel, R. W.; Christerson, A.; Martensson, E.; Onneby, C.; Schadler, L. S. *Nanotechnology* **2005**, *16*, 724−731.

(9) Huang, X.; Kim, C.; Ma, Z.; Jiang, P.; Yin, Y.; Li, Z. *J. Polym. Sci., Polym. Phys.* **2008**, *46*, 2143−2154.

(10) Mukherjee, N.; Wavhal, D.; Timmons, R. B. *ACS Appl. Mater. Interfaces* **2010**, *2*, 397−407.

(11) Thomas, S.; Raman, S.; Mohanan, P.; Sebastian, M. T. *Compos., Part A* **2010**, *41*, 1148−1155.

(12) Lu, X.; Laroussi, M. *J. Phys. D: Appl. Phys.* **2006**, *39*, 1127−1131.

(13) Tsakadze, Z. L.; Ostrikov, K.; Long, J. D.; Xu, S. *Diam. Relat. Mater.* **2004**, *13*, 1923−1929.

(14) Cvelbar, U.; Pejovnik, S.; Mozetic, M.; Zalar, A. *Appl. Surf. Sci.* **2003**, *210*, 255−261.

(15) Shashurin, A.; Shneider, M. N.; Dogariu, A.; Miles, R. B.; Keidar, M. *Appl. Phys. Lett.* **2009**, *94*, 231504.

(16) Levchenko, I.; Huang, S. Y.; Ostrikov, K.; Xu, S. *Nanotechnology* **2010**, *21*, 025605.

(17) Jang, Y. T.; Ahn, J. H.; Ju, B. K.; Lee, Y. H. *Solid State Commun.* **2003**, *126*, 305−308.

(18) Cui, N. Y.; Brown, N. M. D. *Appl. Surf. Sci.* **2002**, *189*, 31−38.

(19) France, R. M.; Short, R. D. *Langmuir* **1998**, *14*, 4827−4835.

(20) Ostrikov, K. N.; Yu, M. Y. *IEEE Trans. Plasma Sci.* **1998**, *26*, 100−103.

(21) Vladimirov, S. V.; Ostrikov, K. N.; Yu, M. Y.; Stenflo, L. *Phys. Rev. E* **1998**, *58*, 8046−8048.

(22) Fortov, V. E; Ivlev, A. V.; Khrapak, S. A.; Khrapak, A. G.; Morfill, G. E. *Phys. Rep.* **2005**, *421*, 1−103.

(23) Xiong, Q.; Lu, X. P.; Ostrikov, K.; Xian, Y.; Zou, C.; Xiong, Z.; Pan, Y. *Phys. Plasmas* **2010**, *17*, 043506.

(24) Lu, X.; Jiang, Z.; Xiong, Q.; Tang, Z.; Pan, Y. *Appl. Phys. Lett.* **2008**, *92*, 151504.

(25) Thierry, B.; Jasieniak, M.; de Smet, L.; Vasilev, K.; Griesser, H. J. *Langmuir* **2008**, *24*, 10187−10195.

(26) Vasilev, K.; Michelmore, A.; Martinek, P.; Chan, J.; Sah, V.; Griesser, H. J.; Short, R. D. *Plasma Process. Polym.* **2010**, *7*, 824−835.

(27) Torchinsky, I.; Rosenman, G. *Nanoscale Res. Lett.* **2009**, *4*, 1209−1217.

(28) Chan, C. M.; Ko, T. M.; Hiraoka, H. *Surf. Sci. Rep.* **1996**, *24*, 3−54.

(29) Nelson, J. K.; Hu, Y. *J. Phys. D: Appl. Phys.* **2005**, *38*, 213−222.

(30) Dissado, L. A.; Fothergill, J. C. In *Electrical Degradation and Breakdown in Polymers*, 1st ed.; Morgan, D. V., Parkman, N., Overshott, K., Eds.; Peter Peregrinus: London, 1992; Vol. 9, p 287−311.

(31) Blom, P. W. M.; Mihailetchi, V. D.; Koster, L. J. A.; Markov, D. E. *Adv. Mater.* **2007**, *19*, 1551−1566.

(32) Dissado, L. A.; Sweeney, P. J. J. *Phys. Rev. B* **1993**, *48*, 16261−16268.

(33) Artbauer, J. *J. Phys. D: Appl. Phys.* **1996**, *29*, 446−456.

(34) Kim, S. H.; Chung, J. W.; Kang, T. J.; Kwak, S. Y.; Suzuki, T. *Polymer* **2007**, *48*, 4271−4277.

(35) Wang, Z. F.; Wang, B.; Qi, N.; Zhang, H. F.; Zhang, L. Q. *Polymer* **2005**, *46*, 719−724.

(36) Bamford, D.; Jones, M.; Latham, J.; Hughes, R. J.; Alam, M. A.; Stejny, J.; Dlubek, G. *Macromolecules* **2001**, *34*, 8156−8159.

(37) Dlubek, G.; Stejny, J.; Lupke, T.; Bamford, D.; Petters, K.; Hubner, C.; Alam, M. A.; Hill, M. J. *J. Polym. Sci., Part B: Polym. Phys.* **2002**, *40*, 65−81.

(38) Lim, S. Y.; Sahimi, M.; Tsotsis, T. T.; Kim, N. *Phys. Rev. E* **2007**, *76*.

(39) Bausch, M. J.; Guadalupefasano, C.; Peterson, B. M. *J. Am. Chem. Soc.* **1991**, *113*, 8384−8388.

(40) Zhang, X. A. *J. Mol. Struct.* **2010**, *981*, 153−158.